Electric-field-induced antiferroelectric to ferroelectric phase transition in mechanically confined $Pb_{0.99}Nb_{0.02}[(Zr_{0.57}Sn_{0.43})_{0.94}Ti_{0.06}]_{0.98}O_3$

X. Tan,[1,*] J. Frederick,[1] C. Ma,[1] E. Aulbach,[2] M. Marsilius,[2] W. Hong,[3] T. Granzow,[2] W. Jo,[2] and J. Rödel[2]
[1]*Department of Materials Science and Engineering, Iowa State University, Ames, Iowa 50011, USA*
[2]*Institute of Materials Science, Technische Universität Darmstadt, 64287 Darmstadt, Germany*
[3]*Department of Aerospace Engineering, Iowa State University, Ames, Iowa 50011, USA*
(Received 31 October 2009; published 5 January 2010)

The electric-field-induced phase transition was investigated under mechanical confinements in bulk samples of an antiferroelectric perovskite oxide at room temperature. Profound impacts of mechanical confinements on the phase transition are observed due to the interplay of ferroelasticity and the volume expansion at the transition. The uniaxial compressive prestress delays while the radial compressive prestress suppresses it. The difference is rationalized with a phenomenological model of the phase transition accounting for the mechanical confinement.

DOI: 10.1103/PhysRevB.81.014103 PACS number(s): 77.65.−j, 77.80.B−, 77.84.Ek, 81.30.Hd

I. INTRODUCTION

Antiferroelectric ceramics can undergo a phase transition into a polar state with parallel oriented dipoles when subjected to strong external electric fields.[1–6] Such a phase transition can even be realized with the intrinsic interfacial field in very thin antiferroelectric films.[7] On the other hand, certain ferrroelectric ceramics can be depolarized and transformed into an antiferroelectric phase by hydrostatic pressures or uniaxial compressive stresses.[1,8–11] These phase switchings involve the development/release of a large electrical polarization and are generally accompanied by a significant volume expansion/contraction, making them the physics basis for many engineering applications. The coupled changes in polarization and volume at the phase transition render these materials responsive to multiple stimuli. However, there are very limited reports in the literature dealing with this matter.[12,13] In the present work, the effect of uniaxial as well as radial compressive prestresses on the electric-field-induced phase transition was investigated in the antiferroelectric $Pb_{0.99}Nb_{0.02}[(Zr_{0.57}Sn_{0.43})_{0.94}Ti_{0.06}]_{0.98}O_3$ (PNZST43/6/2) ceramic with a unique loading fixture we developed recently.[14–16] Considering the different stages in the electric-field-induced phase-transition process, the mechanical confinements are expected to generate ferroelastic domain switching in the antiferroelectric phase before the transition, to suppress the phase transition through acting against volume expansion, to influence the ferroelastic domain switching and to affect the polarization through the direct piezoelectric effect in the induced polar state after the transition.

II. EXPERIMENTAL PROCEDURE

Bulk ceramic of PNZST43/6/2 was synthesized using the conventional solid-state reaction method.[6] After sintering, two types of samples were prepared. For the uniaxial prestress test, a disk sample with diameter of 7.0 mm and thickness of 1.0 mm was prepared with cutting, polishing, and lapping. The whole circular faces of the disk sample were electroded with Ag films by sputtering. The experimental setup for the polarization hysteresis loop measurement under uniaxial compressive prestresses is schematically shown in Fig. 1(a). For the radial prestress test, a cylindrical sample with diameter of 5.9 mm and height of 3.0 mm was electroded with Ag films on the two flat circular end faces. The sample was then loaded into a fixture depicted in Fig. 1(b), which consists of a stiff cylindrical steel housing containing a tightly fit high-density polyethylene tube.[14,15] Under both mechanical confinements, bipolar electric fields with a peak value of 60 kV/cm were applied along the axial direction to trigger the phase transition. The applied field took a triangular wave form with a frequency of 0.05 Hz and the polarization vs electric-field hysteresis loop was used to reveal the phase transition.

III. RESULTS AND DISCUSSION

Under mechanically free conditions, the volume expansion at the electric-field-induced phase transition was confirmed with the simultaneous measurement of the longitudinal axial strain x_{33} and the transverse radial strain x_{11} from a disk sample.[17] As shown in Fig. 2(a), the electric-field-induced phase transition occurs at the critical field E_F of 42.5 kV/cm and the induced polar state returns to the antiferro-

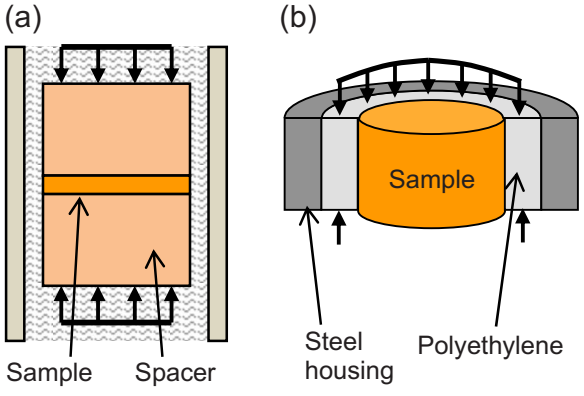

FIG. 1. (Color online) The schematic of the loading fixtures for compressive prestresses: (a) uniaxial and (b) radial.

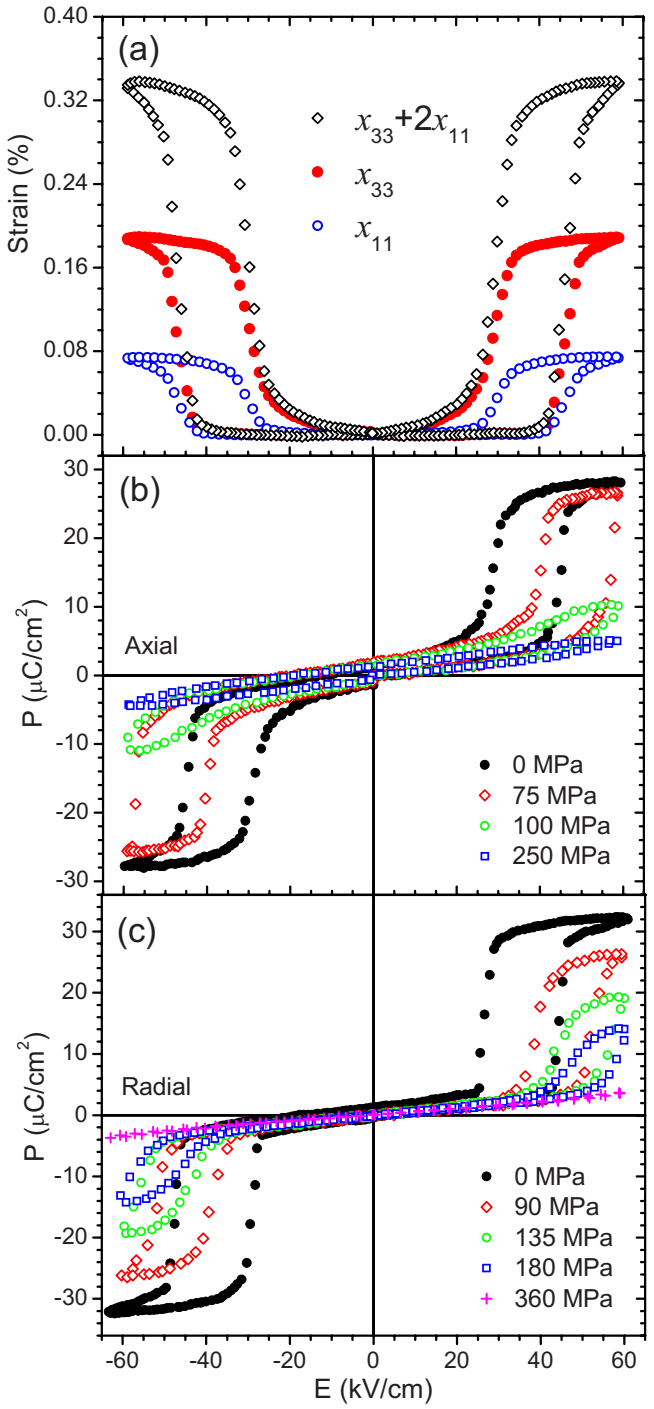

FIG. 2. (Color online) (a) The longitudinal axial strain x_{33}, transverse radial strain x_{11}, and volume strain $(x_{33}+2x_{11})$ measured from a disk sample under no mechanical prestresses. (b) The polarization vs electric-field hysteresis loops under uniaxial compressive prestresses. (c) The hysteresis loops under radial compressive prestresses.

electric phase at E_A of 25.3 kV/cm. At the peak field of 60 kV/cm, x_{33} of 0.189%, x_{11} of 0.075%, and volume strain $(x_{33}+2x_{11})$ of 0.338% were recorded.

The impact of mechanical confinements on the electric-field-induced phase transition was evaluated by monitoring the change in the polarization hysteresis loop. The results for

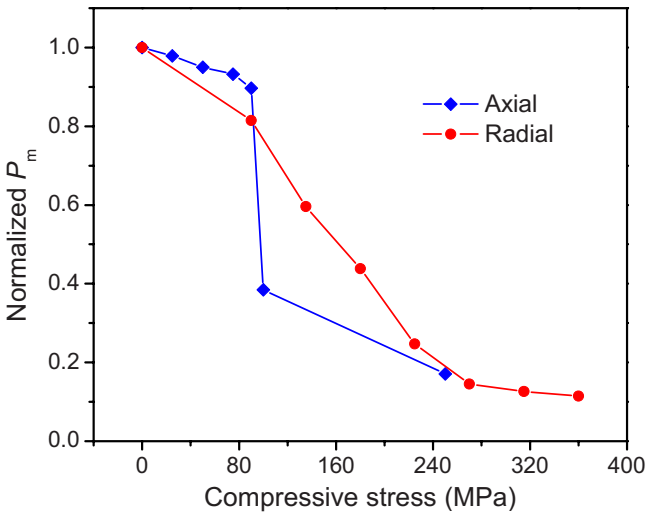

FIG. 3. (Color online) The relative change in maximum polarization P_m under uniaxial and radial compressive prestresses.

the uniaxial compressive prestress condition are displayed in Fig. 2(b). Under the uniaxial compressive stress up to 90 MPa, the prestress delays the phase transition to higher critical fields while it maintains the maximum polarization P_m largely unchanged. The critical field E_F increases at a rate of 0.18 kV/cm per MPa. The almost unchanging P_m indicates that the electric-field-induced phase transition is completed in the whole volume of the sample. At the prestress of 100 MPa, the phase transition is significantly suppressed, manifested by a much reduced P_m of 10.8 $\mu C/cm^2$. Further increase in the prestress to 250 MPa completely prevents the phase transition from occurring and pushes the critical field E_F for the phase transition beyond the applied peak field of 60 kV/cm.

The radial compressive prestress appears to have distinct influences on the field-induced phase transition. As can be seen in Fig. 2(c), the maximum polarization P_m progressively decreases as the radial prestress increases. This indicates that only a fraction of the ceramic sample experiences the phase transition and this fraction gradually becomes smaller as the prestress increases. The critical field E_F also increases with the radial prestress, but at a much slower rate of 0.05 kV/cm per MPa.

The distinct impacts of the two mechanical constraints on the electric-field-induced phase transition can be better appreciated when normalized P_m (with respect to the P_m at 0 MPa) is plotted against the prestress magnitude (Fig. 3). It is evident that the electric-field-induced polarization P_m changes abruptly under the uniaxial prestress condition at 100 MPa (the critical field E_F approaches the applied peak field) but gradually under the radial prestress condition.

The distinct impacts of mechanical confinements on the phase transition warrant further analysis. It is not likely to be caused by the sample geometric effect or the loading fixture because the two types of samples have similar dimensions ($\phi 7.0\times 1.0$ mm^2 vs $\phi 5.9\times 3.0$ mm^2). Furthermore, the deviation in radial stress from constant value during phase transition is estimated to be less than 2% (it is therefore neglected in the subsequent theoretical treatment of the

problem). Under the testing conditions used in the present study, the applied prestress influences the antiferroelectric phase before the transition and the polar phase after the transition due to ferroelastic deformation, and the phase transition itself due to the associated volume expansion.

Prior to the phase transition in the antiferroelectric phase, non-180° antiferroelectric domains are simultaneously ferroelastic domains. It was observed previously that ferroelastic domain switching in antiferroelectric ceramics starts at a uniaxial compressive stress as low as 20 MPa.[18] Under uniaxial compressive stresses, the *c* axis of the orthorhombic unit cell of the antiferroelectric phase is aligned along the loading axis.[11] This *c* axis is the $\langle 001\rangle_c$ (the subscript c indicates the parent cubic perovskite structure) direction. In the antiferroelectric phase Pb^{2+} displaces along the $\langle 110\rangle_c$ direction, generating the antiparallel local dipole moments.[3–5] Hence, prior to the phase transition, the local dipoles are all aligned by the uniaxial compressive prestress in the plane perpendicular to the axial direction. However, the situation is different under the radial compressive prestress. In this case, the $\langle 001\rangle_c$ direction (the orthorhombic *c* axis) will be directed along the radial directions and the local dipole-moment direction $\langle 110\rangle_c$ is expected to be preferentially oriented along the axial direction through ferroelastic domain switching. These different textures in the antiferroelectric phase developed under mechanical prestresses have been confirmed by our x-ray diffraction experiments. It is important to note that the mechanical load does not lead to a transition from the antiferroelectric to the paraelectric phase in PNZST43/6/2. This was confirmed by measurements of the dielectric permittivity under axial loads, where no anomaly was observed in the load range between 0 and 250 MPa.

During the electric-field-induced phase transition, the antiferroelectric phase is transformed into a rhombohedral phase with parallel dipole moments along the $\langle 111\rangle_c$ direction[3,4] accompanied by a volume expansion [Fig. 2(a)]. Under the uniaxial prestress condition, the electric-field-induced phase transition is accomplished largely through a uniform polarization rotation of ~35° *toward* the field direction (from $\langle 110\rangle_c$ to $\langle 111\rangle_c$). While under radial prestresses, the $\langle 110\rangle_c$ was aligned to the field direction in the antiferroelectric phase. The electric-field-induced phase transition is to rotate the polarization *away* from the field direction. Furthermore, the hydrostatic component of the applied compressive stresses acts against the phase transition due to the associated volume expansion. At the same applied stress, the hydrostatic stress in the radial prestress condition would be twice as large as in the uniaxial prestress condition.

After the transition into the induced polar state, the polar domains are aligned by the applied electric field.[4] The concurrent mechanical stress provides an extra driving force for either alignment (radial stress)[14–16] or misalignment (uniaxial stress). Once the polar-domain configuration is fixed, the macroscopic polarization is still affected by the applied stress through the direct piezoelectric effect. Specifically, polarization is reduced by the uniaxial compressive prestress through the piezoelectric coefficient, d_{33}, while enhanced by the radial compressive prestress through the piezoelectric coefficient, d_{31}.[14–16]

To describe the electric-field-induced phase transition under mechanical confinements further, we invoke the Gibbs free energy $\hat{W}$, and write it into three parts

$$\hat{W}(\mathbf{P},\bar{\mathbf{P}},\mathbf{X}) = W_p(\mathbf{P},\bar{\mathbf{P}}) - \hat{W}_e(\mathbf{X}) - \hat{W}_c(\mathbf{P},\bar{\mathbf{P}},\mathbf{X}), \tag{1}$$

where W_p is the free energy of polarization, $\hat{W}_e$ is the complementary strain energy, and $\hat{W}_c$ characterizes the coupling between the stress field $\mathbf{X}$ and the polarizations $\mathbf{P}$ and $\bar{\mathbf{P}}$. Following Cross,[19,20] we represent the polarization state by the ferroelectric polarization $\mathbf{P}$ and the antiferroelectric polarization $\bar{\mathbf{P}}$, and adopt the polarization-energy function in the following form:

$$W_p(\mathbf{P},\bar{\mathbf{P}}) = AP^2 + B\bar{P}^2 + C(P^4 + \bar{P}^4 + 6P^2\bar{P}^2), \tag{2}$$

where $P^2 = P_iP_i$ and $\bar{P}^2 = \bar{P}_i\bar{P}_i$ with the repeated indices representing a summation. Assuming that the coupling energy $\hat{W}_c$ only depends on the invariants, X_{ii}, P^2, $\bar{P}^2$, $P_iX_{ij}P_j$, and $\bar{P}_iX_{ij}\bar{P}_j$, we take the leading order terms and write it in the form

$$\hat{W}_c(\mathbf{P},\bar{\mathbf{P}},\mathbf{X}) = \alpha P_iX_{ij}P_j + \beta\bar{P}_iX_{ij}\bar{P}_j + \gamma X_{ii}P^2. \tag{3}$$

The first term in Eq. (3) represents the complementary strain energy induced through ferroelastic domain switching in the induced polar state, the second term is from the shape change due to the antiferroelectric ferroelastic domain switching, and the last term arises from the significant volume increase during the phase transition. A term in the form of $X_{ii}\bar{P}^2$ is neglected from Eq. (3) after comparison with experimental data. In the following description, we will assume that polarization and electric field are aligned and lie in the 3-direction, and we will just represent them with their magnitudes. We also assume a homogeneous deformation with no shear, so that only X_{11}, X_{22}, and X_{33} are present. Substituting Eqs. (2) and (3) into Eq. (1) and taking derivatives with respect to the polarization and stress, we have the constitutive relations for the electric field

$$E = 2(A + 2CP^2 + 6C\bar{P}^2 - \gamma X_{ii} - \alpha X_{33})P, \tag{4}$$

and the normal strain components

$$x_{11} = x_{22} = x^e_{11} + \gamma P^2 - x^0_{11}$$

$$\text{and} \quad x_{33} = x^e_{33} + (\alpha+\gamma)P^2 + \beta\bar{P}^2 - x^0_{33}, \tag{5}$$

where $x^e_{ij} = \partial\hat{W}_e/\partial X_{ij}$ is the elastic response of the applied stress, and x^0_{ij} is the strain at the reference state in which we initiate the measurements.

For the system to be in equilibrium, the antiferroelectric polarization, as an internal variable, needs to satisfy $\partial\hat{W}/\partial\bar{P} = 0$, and thus

$$2(B + 2C\bar{P}^2 + 6CP^2 - \beta X_{33})\bar{P} = 0. \tag{6}$$

Just as in the two sublattice model,[19] Eq. (6) leads to two branches, differ in $\bar{P}$ values. When $B + 6CP^2 - \beta X_{33} < 0$, $\bar{P}$ has nonzero values given by $\bar{P}^2 = (\beta X_{33} - B)/2C - 3P^2$, and

the ceramic is in an antiferroelectric phase. The corresponding strain can be obtained from Eq. (5)

$$x_{11} = x_{22} = x_{11}^e - x_{11}^0 + \gamma P^2$$

$$\text{and} \quad x_{33} = x_{33}^e - x_{33}^0 + (\alpha + \gamma - 3\beta)P^2 + \frac{\beta(\beta X_{33} - B)}{2C}. \tag{7}$$

When $B+6CP^2-\beta X_{33}>0$, $\bar{P}=0$, and the ceramic is in the field-induced polar state with strain components

$$x_{11} = x_{22} = x_{11}^e - x_{11}^0 + \gamma P^2 \quad \text{and} \quad x_{33} = x_{33}^e - x_{33}^0 + (\alpha + \gamma)P^2. \tag{8}$$

Equations (7) and (8) show that the strain scales with the polarization as P^2. Moreover, the lateral strain components, x_{11} and x_{22}, have the same form in both the antiferroelectric phase and the induced polar phase. On the other hand, the coefficients are different for the axial strain x_{33} in the two phases. These results agree extremely well with the experimental measurements, as shown in Fig. 4(a). From a linear fitting to the data in Fig. 4(a), we find the parameter values: $\gamma \approx 9.3\times10^{-3}$ m^4/C^2, $\alpha \approx 3.8\times10^{-3}$ m^4/C^2, and $\beta B/C \approx -1.7\times10^{-3}$.

When the material is under no mechanical prestresses, the relation between the electric field E and polarization P is fully determined by W_p. Using the data from the stress-free (0 MPa) curves in Figs. 2(b) and 2(c), we find the approximate values for the parameters: $A \approx 0.3$ kV cm/μC, $B \approx -1$ kV cm/μC, and $C \approx 5\times10^{-4}$ kV cm^5/μC^3. Due to the coarse representation of the polarization energy in Eq. (2), the parameters are chosen to give a relation that qualitatively agrees with the experimental curves.

Using the parameters obtained from the stress-free data, we plot Eq. (4) in Fig. 4(b) for the cases when an axial or radial stress is applied, without additional fitting parameters. It can be seen from the plot that the polarization of the upper branch, i.e., the polar phase, is lower when a compressive stress is applied, and the decrease in polarization is more significant when the compression is applied in the radial direction. The agreement with the experimental results confirms the interpretation that the hydrostatic pressure suppresses the volume expansion during the electric-field-induced phase transition. On the lower branch, when the material is antiferroelectric, the critical electric field E_F increases with the applied compressive stress, and the change is more pronounced with the axial compressive stress. This also agrees well with the experimental observation. Limited by the single-crystal model, the transitions in Fig. 4(b) are represented by vertical lines. More realistic transitions can be modeled if grain boundaries and domain walls are considered.

IV. CONCLUSIONS

In summary, the electric-field-induced antiferroelectric to a polar-state phase transition is found to be delayed by uniaxial compressive prestresses and suppressed progressively by radial compressive confinement. Ferroelasticity in both antiferroelectric and field-induced polar phases and the hydrostatic component of the prestresses combine to determine the phase transition and the domain state. The distinct impacts of mechanical confinements on the phase transition are intrinsic to the material, as confirmed by the phenomenological model incorporating the electromechanical coupling.

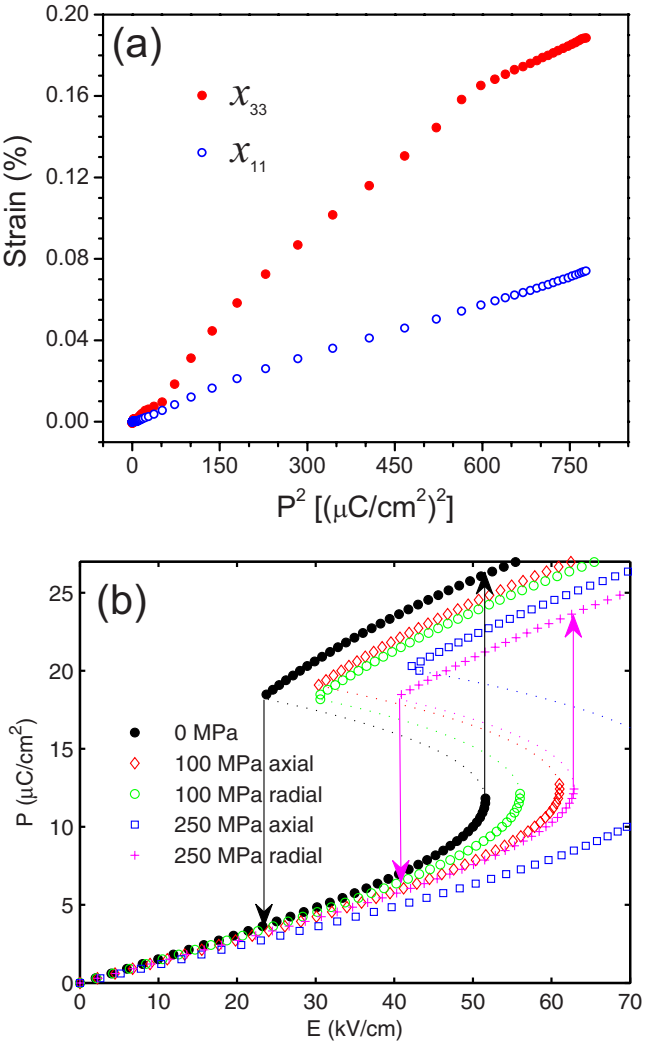

FIG. 4. (Color online) (a) Plot of the strains x_{33} and x_{11} during the loading segment from 0 to 60 kV/cm in Fig. 2(a) as a function of P^2. Note the data were obtained under no prestresses. (b) The model prediction on the relation between the electric field E and the polarization P under various levels of axial and radial compressive prestresses.

ACKNOWLEDGMENTS

This work was supported by the National Science Foundation (NSF) through the CAREER under Grant No. DMR-0346819 and by the Deutsche Forschungsgemeinschaft (DFG) under Grant No. GR2722/4-1.

*Author to whom correspondence should be addressed; xtan@iastate.edu

[1] D. Berlincourt, H. H. A. Krueger, and B. Jaffe, J. Phys. Chem. Solids **25**, 659 (1964).
[2] P. Yang and D. A. Payne, J. Appl. Phys. **71**, 1361 (1992).
[3] C. T. Blue, J. C. Hicks, S. E. Park, S. Yoshikawa, and L. E. Cross, Appl. Phys. Lett. **68**, 2942 (1996).
[4] S. E. Park, M. J. Pan, K. Markowski, S. Yoshikawa, and L. E. Cross, J. Appl. Phys. **82**, 1798 (1997).
[5] H. He and X. Tan, Phys. Rev. B **72**, 024102 (2005).
[6] H. He and X. Tan, J. Phys.: Condens. Matter **19**, 136003 (2007).
[7] P. Ayyub, S. Chattopadhyay, R. Pinto, and M. S. Multani, Phys. Rev. B **57**, R5559 (1998).
[8] I. J. Fritz, J. Appl. Phys. **49**, 4922 (1978).
[9] D. H. Zeuch, S. T. Montgomery, and D. J. Holcomb, J. Mater. Res. **15**, 689 (2000).
[10] M. Avdeev, J. D. Jorgensen, S. Short, G. A. Samara, E. L. Venturini, P. Yang, and B. Morosin, Phys. Rev. B **73**, 064105 (2006).
[11] D. A. Hall, J. D. S. Evans, E. C. Oliver, P. J. Withers, and T. Mori, Philos. Mag. Lett. **87**, 41 (2007).
[12] P. Pertsch, M. J. Pan, F. Chu, and S. Yoshikawa, J. Korean Phys. Soc. **32**, S1286 (1998).
[13] O. Essig, P. Wang, M. Hartweg, P. Janker, H. Nafe, and F. Aldinger, J. Eur. Ceram. Soc. **19**, 1223 (1999).
[14] T. Granzow, A. B. Kounga, E. Aulbach, and J. Rödel, Appl. Phys. Lett. **88**, 252907 (2006).
[15] A. Kounga Njiwa, E. Aulbach, T. Granzow, and J. Rödel, Acta Mater. **55**, 675 (2007).
[16] T. Granzow, Th. Leist, A. B. Kounga, E. Aulbach, and J. Rödel, Appl. Phys. Lett. **91**, 142904 (2007).
[17] X. Tan, W. Jo, T. Granzow, J. Frederick, E. Aulbach, and J. Rödel, Appl. Phys. Lett. **94**, 042909 (2009).
[18] H. Cao and A. G. Evans, J. Am. Ceram. Soc. **76**, 890 (1993).
[19] L. E. Cross, J. Phys. Soc. Jpn. **23**, 77 (1967).
[20] K. Uchino, L. E. Cross, and R. E. Newnham, Jpn. J. Appl. Phys., Part 2 **19**, L425 (1980).